Role of the direct mechanism in dissociative recombination of HCO^+ and HOC^+

Å. Larson* and M. Stenrup
Department of Physics, Stockholm University, S-106 91 Stockholm, Sweden

A. E. Orel
Department of Chemical Engineering and Materials Science, University of California, Davis, California 95616, USA

(Received 4 January 2012; published 2 April 2012)

Studies of the direct mechanism for dissociative recombination of HCO^+ and HOC^+ are presented. The calculations involve wave-packet propagation in three dimensions on electronically resonant states of HCO and HOC with the potential-energy surfaces and autoionization widths obtained from *ab initio* electron scattering and electronic structure calculations. The total cross section and branching ratios for the two molecules and their deuterated isotopologues are calculated and compared to available experiments. The effect of vibrational excitation in DCO^+ has been studied as well.

DOI: 10.1103/PhysRevA.85.042702 PACS number(s): 34.80.Ht, 31.50.Df, 34.80.Lx

I. INTRODUCTION

There are two important mechanisms for collisions of low-energy electrons with molecular ions leading to dissociative recombination (DR). In the direct mechanism originally proposed by Bates [1], an electron recombines with a molecular ion and the kinetic energy of the electron is transferred into electronic excitation forming typically a doubly excited electronic state with a repulsive potential-energy surface. Since the potential energy of this state is above the ionization threshold, there is electronic interaction between the neutral resonant state and the ionization continuum. When the electron is captured, the neutral molecular system can either re-emit the electron (autoionize) or dissociate along the repulsive potential. In the indirect mechanism of DR, first proposed by Bardsley [2], the kinetic energy of the electron is transferred into rovibrational energy of the nuclei, resulting in formation of a rovibrationally excited Rydberg state that subsequently may predissociate. For molecular systems where the potential of the diabatic resonant state crosses the ion potential close to the equilibrium structure, the low-energy DR is driven by the direct mechanism. Other systems do not have such a curve crossing. Recent calculations have shown [3,4] that this is the case of HCO^+.

The formyl cation, HCO^+, is a key ion in interstellar chemistry. Dissociative recombination of this ion has been studied extensively both experimentally and theoretically. The experimental studies [5–20] agree on a relatively large rate of 2×10^{-7} cm^3 s^{-1} at room temperature. Recent measurements [21] of the cross section of DR of $H^{13}CO^+$ found that the cross section at low collision energies falls off like E^{-1} and is followed by a structured high-energy peak centered around 10 eV. Measurements of the branching ratios show that at low collision energies, the HC bond will break [10,20,21]. Using an energy- and position-sensitive surface barrier detector the branching ratios in DR of DCO^+ have recently been measured as a function of the collision energy in the range 0–25 eV at the TSR ion-storage ring at the Max Planck Institute for Nuclear Physics in Heidelberg [22]. These measurements confirmed that at low collision energies, dissociative recombination of DCO^+ is dominated by dissociation into D + CO. For collision energies above 2 eV there is a transition into dissociation to DC + O. The three-body breakup becomes important for collision energies above 6 eV.

Theoretical studies [23–26] show that at low collision energies, the process is driven by the Renner-Teller effect that will induce interactions between the electronic and vibrational motions. The DR process will proceed through recombination into vibrationally excited Rydberg states that subsequently are predissociated. The calculated cross section is a factor of 2 smaller than the measured cross sections at low energies (<0.06 eV) [25]. We have previously [4] combined electron scattering calculations using the complex-Kohn variational method [27] with structure calculations using the multireference configuration interaction (MRCI) technique to compute the potential-energy surfaces and autoionization widths of the electronic resonant states of HCO. We found several resonant states with potential-energy surfaces situated a few eV above the minimum of the ion potential-energy surface. The potentials of the resonant states are repulsive with respect to both radial coordinates and relatively flat with respect to changes in the bending angle. There are clear indications of avoided crossings among the resonant states.

The isoformyl molecular ion, HOC^+, is an isomer of HCO^+ that is 1.72 eV higher in energy and has a barrier to isomerization of 1.61 eV [28]. The ion was first spectroscopically detected in 1982 using laboratory microwave techniques [29]. Since then, it has been observed in interstellar environments in both dense [30,31] and diffuse [32] molecular clouds. In measurements on DR using the flowing afterglow technique [17] or a storage ring [22] both isomers HCO^+ and HOC^+ are believed to be present. However, so far there is no direct measurement nor theoretical computation of the cross section for DR of HOC^+. For the modeling of the chemistry of the afterglow plasma [17], it was assumed that the DR thermal rate coefficients of HCO^+ and HOC^+ are of the same magnitude. For the models of the interstellar chemistry it is assumed that the thermal DR rate coefficient of HOC^+ is 1.3×10^{-7} cm^3 s^{-1} [18,32,33], that is, smaller than that of HCO^+. Our computed resonant states of HOC [4] are lower in energy relative to the ion compared to HCO. Therefore, for

*aasal@fysik.su.se

HOC^+, the direct mechanism of DR might be important even at low collision energies.

We have previously [22] studied the direct mechanism of DR of HCO^+ and HOC^+ using wave-packet propagation on the resonant states including the two radial coordinates and assuming linear geometry. We then focused on the branching ratios and obtained a qualitatively good agreement with the measured branching ratios by assuming a 9% contamination of the HOC^+ ion in the experiment. In the present study, the angle dependences of the potential-energy surfaces are included in the dynamics. We compute not only branching ratios, but also the total cross section from the direct mechanism. We have also performed the wave-packet propagation for deuterated molecular ions. The DCO^+ molecular ion is known to have long-lived excited vibrational states in the bending mode with a lifetime of about 13 s for the (010) state [34]. When this isotopologue is used in the experiment [22], the bending mode is assumed to be vibrationally excited. We have therefore also studied the reaction for vibrationally excited ions. The wave packets are propagated using the MCTDH [35] program developed in Heidelberg.

II. THEORETICAL DETAILS

A. Calculation of potential-energy surfaces and autoionization widths

The details of the computations of the electronic resonant states of HCO and HOC have been outlined in our previous study [4] and hence only a short summary is here presented. The potential-energy surfaces of the electronically bound states are computed using the MRCI method with natural orbitals of the ground state of the ion. In the calculations, the $(1\sigma)(2\sigma)$ core orbitals are kept doubly occupied and the reference configurations are obtained by excitations of 11 electrons (10 for the ion) among eight orbitals. The MRCI wave function is constructed by allowing all single excitations out of the reference configurations. By using the complex-Kohn variational method [27] the energy positions and autoionization widths of the resonant states are determined with the same MRCI wave function for the target ion.

The Rydberg states converging to the ground state of the ion as well as the ionization continuum have the same configuration as the ion plus an outer electron in a diffuse orbital. The resonant states are Rydberg states converging to an excited ionic core. These resonant states all have vacancies in the (5σ) or (1π) molecular orbitals. By following the states with these configurations a quasidiabatization of the resonant states relative to the Rydberg manifold can be performed. In the wave-packet propagation no electronic couplings between the diabatic states are included.

The wave-packet dynamics is performed using internal coordinates. The radial coordinate between H and C (or H and O for HOC) is r_1 and the radial coordinate between C and O is r_2. The angle between the bonds is $\pi - \theta$. In Fig. 1, one-dimensional slices of the potential-energy surfaces of the resonant states of HCO and HOC included in the present study are displayed. The resonant states are shown as a function of the r_2 coordinate for fixed $r_1 = 2.0a_0$ and $\theta = 0^\circ$ (linear geometry). Also the potential of the ion is shown

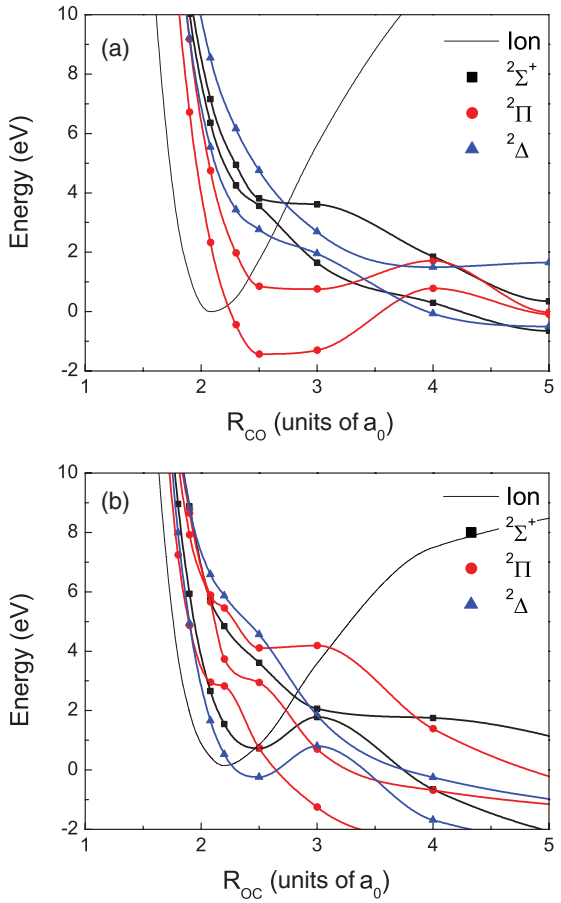

FIG. 1. (Color online) One-dimensional slices of the potential-energy surfaces of the resonant states of (a) HCO and (b) HOC for fixed $r_1 = 2.0a_0$ and $\theta = 0^\circ$. The potential of the ion is also displayed with the thin solid curve. The energy scale is relative to the minimum of the ion potential.

with the black thin curve. For the HCO system, we study the three-dimensional (3D) dynamics for one resonant state of $^2\Sigma^+$ symmetry, two states of $^2\Pi$ symmetry, and one state of $^2\Delta$ symmetry. Furthermore, two-dimensional (2D) results from one additional $^2\Sigma^+$ state and one state of $^2\Delta$ symmetry are included. For HOC, the 3D dynamics is explored for two resonant states of $^2\Pi$ symmetry and one state of $^2\Delta$ symmetry. 2D results from two states of $^2\Sigma^+$ symmetry and one additional state of each of the $^2\Pi$ and $^2\Delta$ symmetries are included. The higher electronic resonant states are difficult to follow when the molecular system becomes bent. Moreover, the cross sections from the higher electronic states are smaller than the cross sections from the low-lying electronic states. Therefore the full 3D dynamics is explored only for the lower-lying resonant states.

B. Extrapolation and fitting of surfaces and widths

The computational effort in theoretical studies of DR increases significantly with the size of the system. Going from a diatomic (1D) system to a triatomic (3D) system might look like a trivial extension. However, one of the most time-consuming steps in these types of calculations are the computations of the potential-energy surfaces and widths of

the resonant states. These electronic states are highly excited and a consistent diabatization is needed when all three internal degrees of freedom are varied. We have here extended our previously calculated [4] potentials and widths in order to describe the three-dimensional dynamics and the breaking of both bonds. The wave-packet propagation technique using the MCTDH method [35] requires that all terms of the Hamiltonian are fitted to the product form

$$V(r_1,r_2,\theta) = \sum_{i,j,k} c_{ijk} v_i(r_1) u_j(r_2) f_k(\theta). \quad (1)$$

Using the POTFIT program in the MCTDH package, the potential-energy surfaces and widths can efficiently be fitted to the desired format provided they are computed on a product grid. This is not done in the present study. The potential surfaces are calculated on a product grid for $1.5a_0 \leqslant r_1 \leqslant 10.0a_0$ and $1.0a_0 \leqslant r_2 \leqslant 10.0a_0$ for the linear geometries $\theta = 0^\circ$. When the system is nonlinear and belongs to the C_s point group, the computational effort of the structure calculations increases since the numbers of configurations in the two irreducible representations A' and A'' become large. The angle dependencies of the surfaces are calculated in the Franck-Condon region and along the "valleys" where one of the bonds will break and the other distance is fixed at the equilibrium distance of the ion. This is justified from our preliminary two-dimensional studies, where we noticed that below 6 eV the two-body breakups dominate [22]. We assume that the potential-energy surfaces can be fitted to the form

$$V(r_1,r_2,\theta) = V_1(r_1,r_2) + V_2(r_1,r_2,\theta). \quad (2)$$

Here $V_1(r_1,r_2)$ is the two-dimensional surface obtained when $\theta = 0^\circ$. This surface is fitted using the POTFIT program. The second term goes to zero when $\theta \to 0$ and it is assumed to have the form

$$V_2(r_1,r_2,\theta) = V_{21}(r_1,\theta) + V_{22}(r_2,\theta). \quad (3)$$

Here $V_{21}(r_1,\theta)$ describes the θ dependence of the surface along the valley when r_2 has the equilibrium distance r_2^e. The shape of V_{22} is determined simply as

$$V_{22}(r_2,\theta) = V_2\left(r_1^e,r_2,\theta\right) - V_{21}\left(r_1^e,\theta\right). \quad (4)$$

Both two-dimensional functions V_{21} and V_{22} are fitted using POTFIT.

We are not able to perform electron scattering calculations at the same level of accuracy when the molecule is bent as for linear geometries. We performed some calculations using a smaller reference space and found that the autoionization widths do not have any strong angle dependence close to the equilibrium structures of the ions. We therefore assume that the autoionization widths are independent of the bending angle and the two-dimensional functions for the widths $\Gamma(r_1,r_2)$ are calculated on a product grid and fitted using the POTFIT program. When the potentials of the resonant states cross the ion potential the autoionization widths are set equal to zero.

C. MCTDH wave-packet propagation

The DR process is studied using wave-packet propagation by a direct integration of the time-dependent Schrödinger equation,

$$i\frac{\partial\Psi}{\partial t} = \left[\hat{T} + V - i\frac{1}{2}\Gamma\right]\Psi. \quad (5)$$

Here V and Γ are the potential-energy surface and autoionization width of the resonant state. In the present wave-packet study the direct DR mechanism is explored and no couplings (electronic nor nonadiabatic) are included among the neutral states. Then the dynamics for each resonant state can be studied separately and the computed cross sections are added together. The autoionization from each resonant state is included using the local approximation [36], where it is assumed that the total energy of the system is high enough for autoionization into a complete set of vibrational levels to be possible. The wave packets are propagated using internal coordinates and zero angular momentum of the molecular system is assumed. The relevant kinetic-energy operator for a triatomic molecule can be found in, e.g., [37] and it has the desired product form necessary for the MCTDH wave-packet propagation. The wave packets are initiated in the resonant states using the initial condition [36]

$$\Psi(t=0) = \sqrt{\frac{\Gamma}{2\pi}}\chi_v. \quad (6)$$

Here, χ_v, is the vibrational wave function of the target ion and is computed using energy relaxation, i.e., propagating the wave packet on the ion potential-energy surface with imaginary time.

In the MCTDH method, the nuclear wave packet is represented as a sum of separable terms with both time-dependent coefficients and single-particle functions [38]. In the present study, ten single-particle functions are used for each internal coordinate of the system. The single-particle functions are represented in terms of a primitive basis. Here a sine basis with 300 basis functions is applied for the two radial coordinates, while a Legendre basis with 60 functions is used for the angular motion. By inserting the expression for the wave function into the time-dependent Schrödinger equation, the MCTDH working equations for the coefficients and single-particle functions can be obtained [38]. The wave packets are propagated using the constant mean-field scheme where the single-particle functions are integrated using the Bulirsch-Stoer extrapolation (BS) scheme of order 7 and an error tolerance of 10^{-6}. For the coefficients, a complex short iterative Lanczos (SIL) algorithm of order 30 is applied, with an error tolerance of 10^{-5}. The wave packets are propagated for the resonant states during 140 fs and the cross section for DR is computed by analyzing the flux absorbed by complex absorbing potentials (CAPs) with strength parameters 0.05 and orders 3, placed at r_1 and $r_2 = 8.0a_0$. The branching ratios (i.e., the separation of the two- and three-body breakup channels) can be computed by projecting the flux onto the bound and continuum vibrational states of the asymptotic potentials [39]. The total cross section for DR from resonant state i is obtained by adding the contributions from all asymptotic vibrational states [40],

$$\sigma_i(E) = \frac{2\pi^3}{E} g_i \sum_{v'} |S_{v'}(E)|^2 . \quad (7)$$

Here, g_i is the ratio of multiplicity of the neutral state to the ionization continuum and $|S_{v'}(E)|^2$ is the transition probability to a specific asymptotic vibrational state v'.

III. RESULTS AND DISCUSSION

A. HCO

In our previous study [22] of DR of HCO^+ we only considered the two radial coordinates in the wave-packet propagation. We here include all three internal coordinates for the lower resonant states. First we illustrate the effect of the bending by comparing the cross sections for the lowest resonant state of $^2\Pi$ symmetry. This is the resonant state that has the largest contribution to the total cross section. As can be seen in Fig. 2, the cross section obtained using the 2D model is peaked around 1.6 eV and has some sharp structures at lower energies. When the molecule becomes bent, the $1\,^2\Pi$ state splits up into two components, A' and A'', with different potential-energy surfaces. The cross section from the $1^2\Pi$ state is given by the sum of the cross sections from the two components. As can be seen, the 3D model provides a cross section with less structures. Furthermore, the direct mechanism now also contributes to the low-energy cross section. This can be explained by the repulsive potential-energy surfaces of the resonant states as a function of θ. Thus the 3D target wave function allows for capture into the resonant state at low energies. It should be noted, however, that the contribution to the low-energy cross section from the direct mechanism is only 17% of the cross section from the indirect mechanism at 0.13 eV [25].

The computed cross sections for all included resonant states are displayed in Fig. 3. The thick curve is the total cross section for direct DR of HCO^+ obtained when adding all contributions. Below 5 eV the resonant states of $^2\Pi$ symmetry dominate the direct DR, while at larger energies the resonant states of other symmetries become important. To obtain the total cross section for DR of HCO^+ the contributions from the indirect and direct mechanisms are added together. The result is displayed with the thick black curve in Fig. 4. The thin dashed curve is the low-energy cross section computed by Douguet *et al.* [25] using multichannel quantum defect theory. When the cross section from the indirect mechanism dies out, the cross sections from the resonant states take over, producing a total cross section that is relatively smooth over a wide range of energies. For larger collision energies, capture into higher resonant states not included in the present study will contribute to the total cross section. In the present study resonant states of HCO with vertical energies below 8 eV relative to the minimum of the ion are included. The solid black circles show the cross section measured using the single-pass merged beam technique [19] and the red open squares show the cross section from a more recent measurement using the CRYRING ion-storage ring [21].

The theoretical cross section has a reasonable agreement with the measured cross section by Le Padellec *et al.* [19], but it does not show the same structured peak above 3 eV obtained with the storage ring experiment [21]. The cross sections from the $^2\Sigma^+$ and $^2\Delta$ resonant states are peaked at this energy, but their magnitudes are considerably smaller than the measured cross section of the high-energy peak. The $1^2\Pi$ resonant state contributes to the cross section with a broad

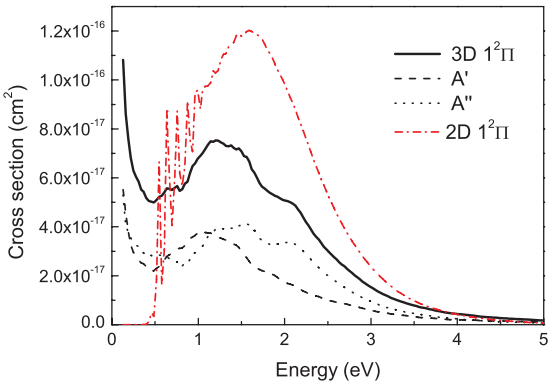

FIG. 2. (Color online) Computed cross section for DR through the $1\,^2\Pi$ resonant state of HCO. The 3D cross section shown with the solid black curve is obtained by adding the contributions from the A' and A'' components of the resonant state (displayed with dashed and dotted curves respectively). The red dashed-dotted curve shows the corresponding 2D cross section.

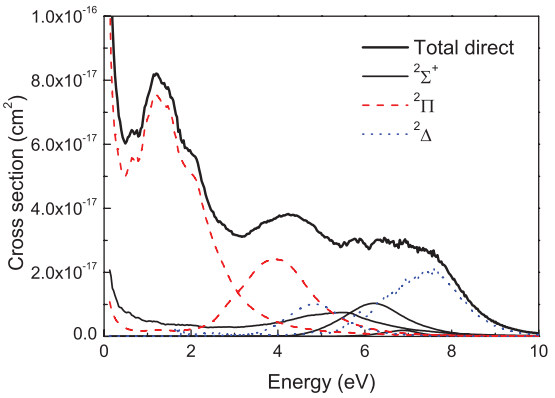

FIG. 3. (Color online) Cross section for direct DR of HCO^+ is displayed with the thick curve. The thin curves show the contributions from the individual resonant states with different electronic symmetries.

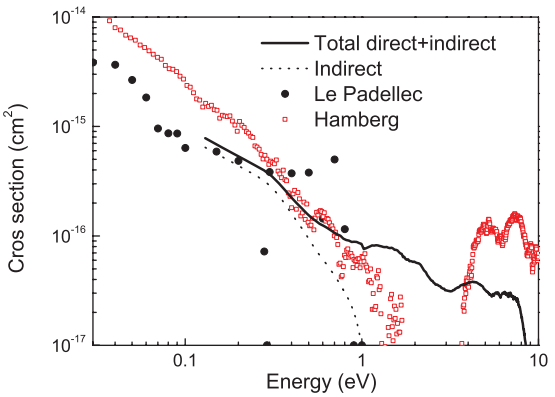

FIG. 4. (Color online) Cross sections for direct and indirect DR of HCO^+ are added and displayed together with the cross section obtained when the electron recombination goes through the Rydberg states (indirect mechanism) [25]. Measured results [19] and [21] are also shown.

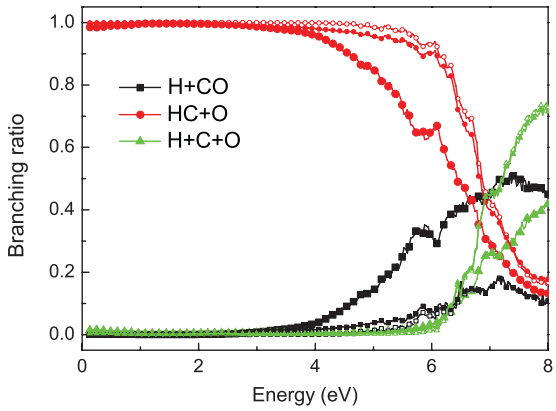

FIG. 5. (Color online) Computed branching ratios for DR of HCO^+ (large filled symbols) as well as DCO^+ in the ground vibrational state (000) (small open symbols) and first excited vibrational state (010) (small filled symbols).

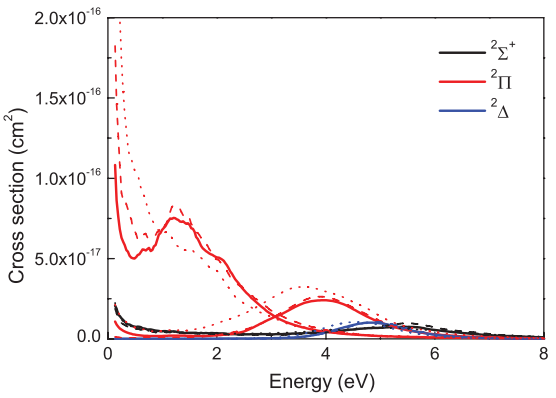

FIG. 6. (Color online) Cross sections for direct DR of $HCO^+(000)$ (solid curves), $DCO^+(000)$ (dashed curves), and $DCO^+(010)$ (dotted curves).

peak around 1.5 eV. The storage ring cross section is very small in this region. In the background subtraction procedure of measurement [21] it was assumed that the detected signal at 2.0 eV completely originated from background events.

By projecting the flux absorbed by the CAPs onto the vibrational states of the asymptotic potentials, the branching ratios can be computed. Here we have not considered the possibility that if both bonds break the angle between the bonds might be small enough to form a bond between H and O. The resulting branching ratios are displayed with large filled symbols in Fig. 5. When computing these branching ratios, the low-energy cross section from the indirect capture into the Rydberg states is not included. It is known that at low collision energies, the HC bond will break yielding H + CO. However, as soon as the direct capture into the resonant states takes over, there will be a complete transition to dissociation into HC + O. Above 4 eV the branching ratio for breaking the HC bond starts to increase and three-body breakup becomes important above 6 eV. As mentioned above, in the present model no couplings between the neutral states are included. How these couplings might influence the branching ratios will be examined further in Sec. III E.

B. DCO

By changing the atomic mass in the wave-packet relaxation and propagation, DR of DCO^+ can be investigated. Because of the smaller differences in masses between the atoms, the deuterated ion has been used in the storage ring experiment at TSR [22]. Using DCO^+ instead of HCO^+ the risk that the light atom will miss the detector is reduced. In Fig. 6, the cross sections for direct DR of DCO^+ and HCO^+ are compared for the resonant states included in the 3D model. Since for these resonant states, the wave-packet dynamics is dominated by the breaking of the CO bond, the change of reduced mass for the deuterated ion has no significant effect on the cross section. We find cross sections that are slightly larger for the deuterated ion at the lower energies, probably due to the small contraction of the initial wave function because of the change in the reduced mass.

In Fig. 5 the branching ratios in DR with DCO^+ are displayed with small open symbols. Most notable is the reduced branching ratio for dissociation into D + CO above 4 eV when this channel opens up. This can be explained by the slower nuclear motion for the heavier isotopologue and hence a larger probability for autoionization.

As mentioned above, the DCO^+ ion has very long-lived vibrational states for the bending mode. At the TSR experiment, Coulomb explosion imaging revealed that after 4 s of storage, the vibrational excitation energy of the ions was about 0.2 eV [22]. We have studied DR of DCO^+ in the (010) vibrational state. During relaxation, the first excited eigenstate is computed and this wave function is used for the initial condition of the wave packet in Eq. (6). The resulting cross sections are displayed with dotted curves in Fig. 6. The largest effect from vibrationally excited ions appears in the cross section for the lowest $^2\Pi$ resonant state that now monotonically decreases with increasing energy.

The small filled symbols of Fig. 5 show the branching ratios for DR with $DCO^+(010)$. There is no large difference between the branching ratios for DR of DCO^+ in the ground and first excited vibrational states.

C. HOC

The resonant states of HOC have lower energy relative to the ion compared to HCO. Our previous 2D wave-packet study showed that the $1^2\Delta$ resonant state has the largest contribution to the DR cross section. However, it did not contribute to the cross section at low energies. The 2D model resulted in a sharply peaked structure centered around 0.6 eV. In Fig. 7 we compare cross sections for DR through the $1^2\Delta$ resonant state computed using the 2D and 3D models. Inclusion of the bending allows for capture into the resonant state even at low collision energies. According to the 3D model, the direct mechanism of DR of HOC^+ provides a cross section with about half the magnitude of the the DR cross section of HCO^+ at 0.13 eV (4.2×10^{-16} cm^2 compared with 7.8×10^{-16} cm^2).

In Fig. 8 we show the total cross section for direct DR of HOC^+ with the thick black curve. We also show the contributions to the cross section from the individual resonant states. We have used the 3D model for two states of $^2\Pi$ symmetry and the lowest resonant state of $^2\Delta$ symmetry.

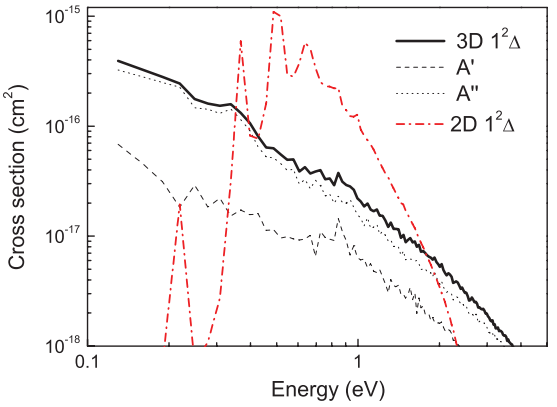

FIG. 7. (Color online) Computed cross section for DR through the $1^2\Delta$ resonant state of HOC using the 3D (black solid curve) and 2D models (red dashed-dotted curve). Also the contributions from the A' and A'' components of the resonant state are displayed with black dashed and dotted curves respectively.

Furthermore we here include the 2D results for two states of $^2\Sigma^+$ symmetry and one additional state of each of the $^2\Pi$ and $^2\Delta$ symmetries. As mentioned before, the low-energy DR is dominated by dissociation through the $1^2\Delta$ resonant state. Above 1 eV there are pronounced structures in the cross section originating from higher resonant states of all symmetries.

The computed branching ratios in DR of HOC^+ are displayed with filled symbols in Fig. 9. It can be noted that the branching ratios for DR of HOC^+ are very different from those of HCO^+. At low energies, the branching ratios are dominated by HO + C dissociation. In the present model the capture into the Rydberg states is not included and this might influence not only the total cross section, but also the branching ratios at low energies. Furthermore, as discussed above, electronic couplings between neutral states can also change the branching ratios. At larger energies also dissociation into H + OC becomes important. There are oscillations in the branching ratios indicating different dissociation dynamics for the contributing resonant states. For energies above 6 eV breaking of both bonds can occur.

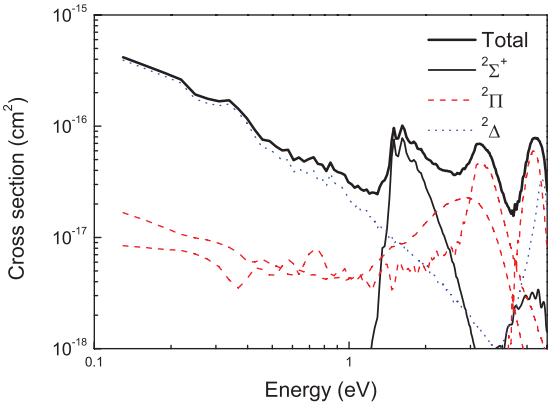

FIG. 8. (Color online) Cross section for the direct mechanism in DR of HOC^+. The contributions from the individual resonant states are displayed with the thin curves.

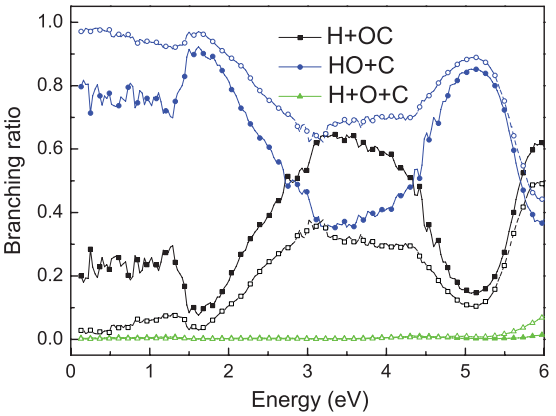

FIG. 9. (Color online) Branching ratios for the direct mechanism in DR of HOC^+ (filled symbols) and DOC^+ (open symbols).

D. DOC

The cross section for direct DR of DOC^+ is computed and displayed with the dashed curve in Fig. 10 together with that of HOC^+. Again we note that the deuterated ion provides a slightly increased (factor of 1.2) cross section at low collision energies due to the contracted target wave function. The branching ratios in direct DR of DOC^+ are displayed with the dashed curves in Fig. 9. The branching ratio for dissociation into D + CO is smaller than the corresponding ratio for H + CO due to the increased mass and slower propagation on the resonant state.

E. Comparison with measured branching ratios

The energy dependence of the branching ratios in DR of DCO^+ has been measured at the TSR ion storage ring using an energy- and position-sensitive surface barrier detector [22]. In the experiment a contamination of 9% DOC^+ ions was assumed. In the theoretical model we assume the same amount of admixture of DOC^+ ions and the resulting calculated branching ratios are displayed in Fig. 11 with filled symbols. At low collision energies we use the cross section for the indirect mechanism from Douguet *et al.* [25] and we assume a complete dissociation into D + CO. The low-energy cross section of DCO^+ is about a factor of 0.7 of

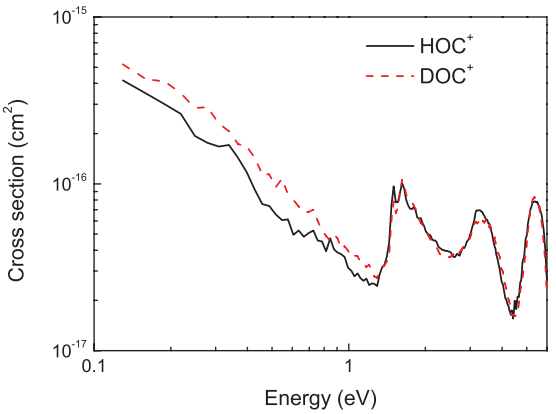

FIG. 10. (Color online) Total cross sections for direct DR of HOC^+ and DOC^+.

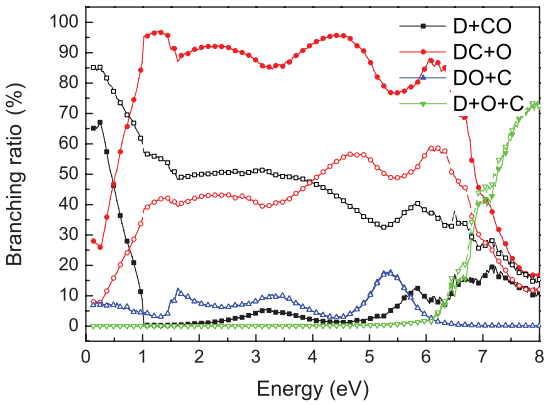

FIG. 11. (Color online) Calculated branching ratios for DR of a DCO^+ ion beam having a 9% admixture of DOC^+ ions (filled symbols). The curves plotted with open symbols show the branching ratios obtained when the electronic couplings between the resonant states and the Rydberg states are considered using the Landau-Zener model.

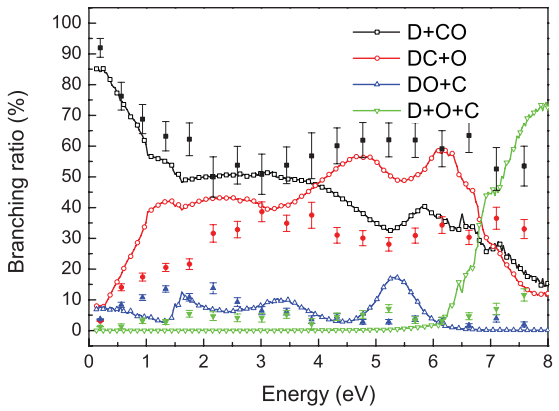

FIG. 12. (Color online) Comparison between measured (large filled symbols) and computed (small open symbols) branching ratios in DR of a DCO^+ ion beam having a 9% admixture of DOC^+ ions. The computed branching ratios are obtained when the electronic couplings between the resonant states and the Rydberg states are considered using the Landau-Zener model.

the cross section of HCO^+ [25] and we have simply scaled the HCO^+ cross section with this factor. Around 0.5 eV there is a transition from dissociation into D + CO to dissociation into DC + O. Then the energy is high enough for electron recombination into the resonant states to take place and the direct mechanism starts to drive the reaction. The breakup into DO + C is a minor channel due to the small contamination of DOC^+ ions. For collision energies above 6 eV the branching ratio for dissociation into D + C + O starts to become important.

As mentioned above, no electronic couplings are included in the present model. After recombination into the resonant state and if the system survives autoionization, the system is assumed to follow the state diabatically without making any transition to other electronic states. This approximation is more justified at higher collision energies where the system will evolve more diabatically on the resonant states. To examine the role of the electronic couplings for the branching ratios we set up a simple model where we redistributed the flux between the neutral states using the Landau-Zener [41] formula for the transition probabilities between diabatic states. In this model we assume that when the system is captured into the resonant state, the CO bond will start to break. On the way out to dissociation, the potential-energy surface crosses Rydberg states and there are probabilities to make transitions to these states. The Rydberg states are closed for dissociation into DC + O. Rather the flux that is transferred will be redistributed into D + CO dissociation.

To estimate the transition probabilities, the electronic coupling strength, the difference in the slopes of the diabatic potentials, as well as the radial velocity at the crossing point have to be known. These parameters are estimated using one-dimensional slices of the potential-energy surfaces of the resonant states and Rydberg states at $r_1 = 2.0a_0$ and $\theta = 0^\circ$ (linear geometry). The electronic couplings are approximated with half of the energy separation between the adiabatic potential-energy surfaces at the avoided crossing. To consider the couplings to the infinite number of Rydberg states not obtained in the structure calculations, effective states [42] are included for all Rydberg series. The resulting branching ratios are shown with the curves with open symbols in Fig. 11. It should be noted that now the importance of the D + CO channel increases at low collision energies and the transition from breaking the DC bond to breaking the CO bond is not as abrupt. In the model no couplings among the DOC electronic states are included, hence it will only affect the D + CO and DC + O branching ratios.

In Fig. 12 the computed branching ratios are compared with the ones measured using the TSR ion storage ring [22]. We here show the computed branching ratios for which dissociating flux is redistributed using the Landau-Zener model. At low energies dissociation into D + CO dominates, but as soon as electron capture into the resonant states becomes energetically feasible, the breakup into DC + O starts to be important. In both the experimental and theoretical results there is some (up to 15%) breakup into DO + C. For collision energies above 6 eV the measured branching ratio for dissociation into D + C + O starts to become important. The same behavior can be seen in the computed branching ratios, even though the theoretical models overestimate the role of three-body breakup at these energies. We believe that one explanation for this is the higher resonant states not included in the present model. By including these states the contribution to the two-body breakups will become more important at larger energies.

IV. CONCLUSION

The role of the direct mechanism in DR of HCO^+ and HOC^+ ions and their deuterated isotopologues have been examined using three-dimensional wave-packet propagation on electronic resonant states.

For HCO^+ we find that the inclusion of the bending angle has effect on the contribution from the lowest resonant $^2\Pi$ state to the cross section at relatively low collision energies. The computed cross section is in good agreement with the merged-beam measurement by Le Padellec *et al.* [19], but it does not reproduce the high-energy peak observed in the more recent cross section measured using the CRYRING storage ring

[21]. Our calculation provides a peak with similar shape and position, but significantly smaller magnitude. When the energy is high enough to capture into the resonant states, the DR of HCO^+ will form HC + O products. For energies above 4 eV, the importance of H + CO increases and above 6 eV, the three-body breakup dominates. The isotope effect at these energies is not significant. The largest change can be seen in the ratio for breakup of the HC bond that decreases for the heavier isotopologue. When the DCO^+ ion is vibrationally excited in the bending mode, the cross sections will increase at lower energies.

In DR of HOC^+ we find that the direct mechanism is important even at low energies. The computed cross section of HOC^+ is about a factor of 2 smaller than the cross section of HCO^+. At low collision energies the resonant states will mainly dissociate into HO + C, but above 2 eV also the breakup into H + OC is important. The three-body breakup increases above 6 eV.

We compare the computed branching ratios for DR of an ion beam of DCO^+ with a 9% admixture of DOC^+ ions with measured branching ratios using the TSR ion storage ring [22]. In order to explain the measured branching ratios, the electronic couplings between the neutral states have to be included. This is illustrated with a simple model where the flux is redistributed using the Landau-Zener formula.

ACKNOWLEDGMENTS

Å.L. acknowledges support from The Swedish Research Council and A.E.O. acknowledges support from the National Science Foundation, Grant No. PHY-08-55092.

[1] D. R. Bates, Phys. Rev. **78**, 492 (1950).
[2] J. N. Bardsley, J. Phys. B **1**, 365 (1968).
[3] Å. Larson, S. Tonzani, R. Santra, and C. H. Greene, J. Phys.: Conf. Ser. **4**, 74 (2005).
[4] Å. Larson and A. E. Orel, Phys. Rev. A **80**, 062504 (2009).
[5] M. T. Leu, M. A. Biondi, and R. Johnsen, Phys. Rev. A **8**, 420 (1973).
[6] B. Ganguli, M. A. Biondi, R. Johnsen, and J. L. Dulaney, Phys. Rev. A **37**, 2543 (1988).
[7] T. Amano, J. Chem. Phys. **92**, 6492 (1990).
[8] N. G. Adams, D. Smith, and E. Alge, J. Chem. Phys. **81**, 1778 (1984).
[9] N. G. Adams and D. Smith, *Molecular Astrophysics. State of the Art and Future Directions. Proceedings of the NATO Advanced Workshop*, edited by G. H. F. Diercksen *et al*. (Reidel, New York, 1985), p. 657.
[10] N. G. Adams, C. R. Herd, M. Geoghegan, D. Smith, A. Canosa, J. C. Gomet, B. R. Rowe, J. L. Queffelec, and M. Morlais, J. Chem. Phys. **94**, 4852 (1991).
[11] N. G. Adams and L. Babcock, Astrophys. J. **434**, 184 (1994).
[12] B. R. Rowe, J. C. Gomet, A. Canosa, C. Rebrion, and J. B. A. Mitchell, J. Chem. Phys. **96**, 1105 (1992).
[13] T. Gougousi, M. F. Golde, and R. Johnsen, Chem. Phys. Lett. **265**, 399 (1997).
[14] J. M. Butler, L. M. Babcock, and N. G. Adams, Mol. Phys. **91**, 81 (1997).
[15] S. Laubé, A. Le Padellec, O. Sidko, C. Rebrion-Rowe, J. B. A. Mitchell, and B. R. Rowe, J. Phys. B **31**, 2111 (1998).
[16] V. Poterya, J. L. McLain, N. G. Adams, and L. M. Babcock, J. Phys. Chem. A **109**, 7181 (2005).
[17] R. E. Rosati, M. P. Skrzypkowski, R. Johnsen, and M. F. Golde, J. Chem. Phys. **126**, 154302 (2007).
[18] I. Korolov, R. Plasil, T. Kotrik, P. Dohnal, and J. Glosik, Int. J. Mass Spectrom. **280**, 144 (2009).
[19] A. Le Padellec, C. Sheehan, D. Taxlbi, and J. B. A. Mitchell, J. Phys. B **30**, 319 (1997).
[20] W. D. Geppert, R. Thomas, A. Ehlerding, J. Semaniak, F. Österdahl, M. af Ugglas, N. Djurić, A. Paál, and M. Larsson, Faraday Discuss. **127**, 425 (2004).
[21] M. Hamberg *et al*. (unpublished).
[22] C. Nordhorn, D. Bing, H. Buhr, M. Grieser, O. Heber, C. Krantz, M. B. Mendes, R. Repnow, D. Schwalm, A. Shornikow, J. Stützel, A. Wolf, O. Novotný, M. Lestinsky, Å. Larson, M. Stenrup, and A. E. Orel, J. Phys.: Conf. Ser. **300**, 012004 (2011).
[23] I. A. Mikhaylov, V. Kokoouline, Å. Larson, S. Tonzani, and C. H. Greene, Phys. Rev. A **74**, 032707 (2006).
[24] N. Douguet, V. Kokoouline, and C. H. Greene, Phys. Rev. A **77**, 064703 (2008).
[25] N. Douguet, V. Kokoouline, and C. H. Greene, Phys. Rev. A **80**, 062712 (2009).
[26] Ch. Jungen and S. T. Pratt, J. Chem. Phys. **129**, 164311 (2008).
[27] T. N. Rescigno, C. W. McCurdy, A. E. Orel, and B. H. Lengsfield III, *The Complex Kohn Variational Method in Computational Methods for Electron-Molecule Scattering*, edited by W. H. Huo and F. A. Gianturco (Plenum, New York, 1995).
[28] M. Mladenović and S. Schmatz, J. Chem. Phys. **109**, 4456 (1998).
[29] C. S. Gudeman and R. C. Woods, Phys. Rev. Lett. **48**, 1344 (1982).
[30] R. C. Woods, C. S. Gudeman, R. L. Dickman, P. F. Goldsmith, G. R. Huguenin, W. M. Irvine, Å. Hjalmorson, L.-Å. Nyman, and H. Olofsson, Astrophys. J. **270**, 583 (1983).
[31] L. M. Ziurys and A. J. Apponi, Astrophys. J. **455**, L73 (1995).
[32] H. Liszt, R. Lucas, and J. H. Black, Astron. Astrophys. **428**, 117 (2004).
[33] The UMIST database; see [www.udfa.net].
[34] M. Heninger, J. Lemaire, S. Fenistein, R. Marx, and G. Mauclaire, Int. J. Mass Spectrom. **185**, 131 (1999)
[35] The MCTDH Package, Version 8.4 (2007); G. A. Worth, M. H. Beck, A. Jäckle and H.-D. Meyer, see [http://mctdh.uni-hd.de], University of Heidelberg, Germany.
[36] C. W. McCurdy and J. L. Turner, J. Chem. Phys. **78**, 6773 (1983).
[37] B. Weis and K. Yamashita, J. Chem. Phys. **99**, 9512 (1993).
[38] M. H. Beck, A. Jäckle, G. A. Worth, and H.-D. Meyer, Phys. Rep. **324**, 1 (2000).
[39] A. Jäckle and H.-D. Meyer, J. Chem. Phys. **105**, 6778 (1996).
[40] D. J. Haxton, Z. Zhang, H.-D. Meyer, T. N. Rescigno, and C. W. McCurdy, Phys. Rev. A **69**, 062714 (2004).
[41] C. Zener, Proc. R. Soc. London A**137**, 696 (1932).
[42] Å. Larson and A. E. Orel, Phys. Rev. A **64**, 062701 (2001).